J. Math. Biol. (2007) 55:721–743
DOI 10.1007/s00285-007-0103-9

Mathematical Biology

A Riemannian manifold analysis of endothelial cell monolayer impedance parameter precision

Anthony E. English · Conrad P. Plaut · Alan B. Moy

Received: 5 October 2006 / Revised: 23 April 2007 / Published online: 14 June 2007

Abstract Endothelial cell adhesion and barrier function play a critical role in many biological and pathophysiological processes. The decomposition of endothelial cell adhesion and barrier function into cell–cell and cell–matrix components using frequency dependent cellular micro-impedance measurements has, therefore, received widespread application. Few if any studies, however, have examined the precision of these model parameters. This study presents a parameter sensitivity analysis of a representative cellular barrier function model using a concise geometric formulation that includes instrumental data acquisition settings. Both model state dependence and instrumental noise distributions are accounted for within the framework of Riemannian manifold theory. Experimentally acquired microimpedance measurements of attached endothelial cells define the model state domain, while experimentally measured noise statistics define the data space Riemannian metric based on the Fisher information matrix. The results of this analysis show that the sensitivity of cell–cell and cell–matrix impedance components are highly model state dependent and several

This work was supported by a National Science Foundation CAREER Award (AE), BES-0238905, and in part by the American Heart Association under Grant 0265029B (AE).

A. E. English (✉)
Department of Mechanical, Aerospace and Biomedical Engineering,
The University of Tennessee, Knoxville, TN 37996, USA
e-mail: tenglish@utk.edu

C. P. Plaut
Department of Mathematics, The University of Tennessee, Knoxville, TN 37996, USA
e-mail: cplaut@utk.edu

A. B. Moy
Cellular Engineering Technologies Inc., Coralville, IA 52241, USA
e-mail: abmoy@mac.com

well defined regions of low precision exist. The results of this study further indicate that membrane resistive components can significantly reduce the precision of the remaining parameters in these models.

Keywords Cell–cell adhesion · Cell–matrix adhesion · Cellular impedance · Endothelial · Information geometry · Biomedical electrodes · Biomedical transducers

Mathematics Subject Classification (2000) 62B10 · 92C37 · 53B21

1 Introduction

The application of microimpedance spectroscopy to the study of endothelial cell adhesion and barrier function has provided valuable insight into a number of biological and pathophysiological processes [6,8,11,13,17,23,24,27,28,30,31,33]. By measuring endothelial cell electrical microimpedances over a range of frequencies, lumped barrier function parameters can be determined by the non-linear optimization of cellular models that include cell–matrix and cell–cell impedance parameters [14,15,18–21]. Although cellular micro-impedance methods have found widespread application in endothelial cell adhesion and barrier function parameter estimation, few if any studies have examined the precision of the parameters [12]. In addition, the precision associated with different combinations of these parameters for a given level of instrumental noise is not often clear.

The non-linearity of the models used to estimate cellular barrier function parameters derived from impedance measurements presents a significant obstacle to quantifying the parameter sensitivity. The parameter sensitivity, correlation, and error can vary from one model state to another and are dependent on instrumental noise levels that can also vary from one data state to another. Geometrically, it is desirable to measure the length and angles between parameter vectors based on instrumental noise levels. This would then allow one to define the separation distance between two parameter states.

Information geometry provides a consistent framework for analyzing model parameter precision and stability based on parameterized sets, or manifolds, of probability distributions [1,3]. Rao first introduced a Riemannian structure on this probability manifold [26]. Subsequent contributions by Csiszar [10], Chentsov [9], and Nagoaka and Amari [22] have led to a mature field that has found applications in neural networks [4,5], statistical physics [29], information science [2], and many other disciplines. In statistics, the Cramer–Rao inequality expresses an upper bound on the precision of a statistical estimator based on the Fisher information. It states that the reciprocal of the Fisher information is a lower bound on the variance of an unbiased parameter estimator. The results of this analysis, therefore, provide an upper bound on the available precision obtainable for a given data sampling and noise level. By also considering the determinant components of the Fisher information matrix, this particular study also sets an upper bound on the obtainable precision for combinations of model parameters.

The central aim of this study is to determine the state dependent precision of different parameter combinations for a given level of instrumental noise and model states using

a representative cellular impedance model in widespread use. To adequately treat the nonlinearity of the problem and account for instrumental noise and data sampling, this study examines the parameter precision from a global geometric point of view. Direct experimental measurements and model simulations provide bounds on the appropriate domain of model states to consider. Frequency dependent noise measurements are then used to estimate the data space Fisher information metric. The parameter precision is then quantified using this metric directly on the data space and by using its pullback on the model space.

2 Model, physical and experimental state spaces

2.1 Problem and model definitions

The primary objective of this study is to quantify cellular model barrier parameter precision in a global geometric context using a representative model and instrumental data acquisition settings. In this particular case, the model system consists of a layer of endothelial cells grown on a microelectrode, as shown in Fig. 1. The frequency dependent impedance is a function of the cell–cell, cell–matrix, and cell membrane impedance components. These impedance components are used to study cellular adhesion and barrier function [20,21]. Increasing cell–cell impedances, for example, are associated with more tightly adhering cell–cell junctions.

Solutions to the specific cellular impedance can be obtained using the continuity arguments outlined in Fig. 1. The explicit function of the distributed model parameters for a circular geometry has been worked out in detail [14,15] and is given by

$$\frac{1}{Z_c} = \frac{1}{Z_n}\left[\frac{Z_n}{Z_n + Z_m} + \frac{\frac{Z_m}{Z_n+Z_m}}{\frac{\gamma r_c}{2}\frac{I_0(\gamma r_c)}{I_1(\gamma r_c)} + R_b\left(\frac{1}{Z_n} + \frac{1}{Z_m}\right)}\right], \tag{1}$$

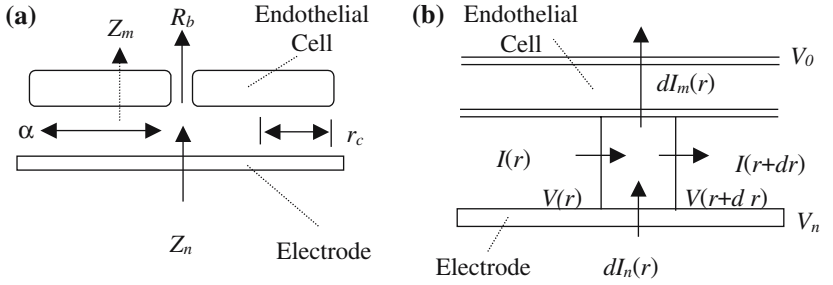

Fig. 1 Bulk electrical parameter and micro-continuum model. **a** The cell covered electrode impedance can be defined as a function of bulk electrical parameters that represent the naked electrode impedance, Z_n, the cell–cell junction impedance, R_b, the membrane impedance, Z_m, and the effective subcellular impedance, α. The term r_c represents the cell radius. **b** The governing partial differential equation is derived from a continuity model where I is the subcellular current, I_n the electrode current, I_m the membrane current, V_n the naked electrode voltage, V_0 the solution voltage, and V the subcellular potential. The term r denotes the radial coordinate

where Z_c is the cell covered impedance, Z_n the naked electrode impedance, Z_m the cell membrane impedance, R_b the cell–cell junction impedance, and $I_0(\gamma r_c)$ and $I_1(\gamma r_c)$ are the modified Bessel functions of the first kind of zero and first order, respectively. The term r_c represents the cell radius and

$$\gamma = \sqrt{\frac{\rho}{h}\left(\frac{1}{Z_n} + \frac{1}{Z_m}\right)}, \tag{2}$$

where ρ is the media resistivity and h is the cell substrate separation distance. The product form γr_c, that appears in Eq. 1, thus becomes

$$\gamma r_c = r_c\sqrt{\frac{\rho}{h}} \cdot \sqrt{\left(\frac{1}{Z_n} + \frac{1}{Z_m}\right)} = \alpha\sqrt{\left(\frac{1}{Z_n} + \frac{1}{Z_m}\right)}, \tag{3}$$

where the additional parameter,

$$\alpha = r_c\sqrt{\frac{\rho}{h}}, \tag{4}$$

represents an effective cell–matrix impedance. The cell membrane resistance, Z_m, can be written as a series combination of the apical and basal membrane impedances, i.e.,

$$Z_m = \frac{2R_m}{1 + \mathrm{j}2\pi f R_m C_m}, \tag{5}$$

where R_m is the membrane resistance, C_m the membrane capacitance, $\mathrm{j} = \sqrt{-1}$, and f is the frequency. In practice, the frequencies, f, and naked electrode impedance, Z_n are assumed known quantities. In the following, the four parameters, α, R_b, C_m, and R_m represent the model parameters to be analyzed using the micro-impedance function Z_c and instrumental noise and data acquisition settings.

2.2 Model, physical, and experimental space coordinates

The set of four parameters $y = (\alpha, R_b, C_m, R_m)$ are the cellular model space coordinates of some open subset M of Euclidean space for which these quantities have physical meaning. For this application, the model space coordinate system implicitly defines the physical units of $\{\alpha, R_b, C_m, R_m\}$ as $\Omega^{0.5}\,\mathrm{cm}$, $\Omega\,\mathrm{cm}^2$, $\mu\mathrm{F}\,\mathrm{cm}^{-2}$, and $\Omega\,\mathrm{cm}^2$, respectively.

For any set $\{f_1, \ldots, f_n\}$ of frequencies, the real and imaginary parts of the n corresponding frequency dependent impedances define a smooth function $Z_c : M \to Z \subset \Re^{2n}$ via Eqs. 1–4. The cellular impedance model function, Z_c, maps each model state y into a physical space element, $z \in Z \subset \Re^{2n}$, of all measurable impedance values. The set of $2n$ coordinates $z = (z^1, \ldots, z^{2n})$ of the physical space represent the $2n$ real and imaginary frequency values of the impedance. In this study, the physical space coordinate system $\{z^a\}$ defines the frequency dependent electrode impedance components in units of $\Omega\,\mathrm{cm}^2$.

The measurement of each impedance state $z \in Z$ produces a statistical distribution of measured values depending on the experimental circuit configuration and the instrument data acquisition settings. A given circuit configuration and instrumental data acquisition settings, therefore, define a map, ϕ, from Z into a statistical manifold $\mathcal{S} = \{p(x, \theta)\}$, where x is a random variable belonging to the sample space $X = \Re^{2n}$, and $p(x, \theta)$ is the probability density function of x, parameterized by θ [1,3]. For the purpose of this study we will assume that each physical impedance value produces a normal distribution of impedance values when it is measured. The manifold $\mathcal{S}$, therefore, consists of all normal probability distribution functions on the sample space $X = \Re^{2n}$ parameterized by a single coordinate chart (Θ, θ) consisting of the components of the mean μ and the components of the upper triangle Δ of the population covariance matrix Σ, i.e.,

$$p(x; \{\mu, \Sigma\}) = (2\pi \det \Sigma)^{-n} \exp\left\{-\frac{1}{2}(x-\mu)^T \Sigma^{-1}(x-\mu)\right\}, \tag{6}$$

where T is the transpose, and the coordinate chart maps $p(x; \{\mu, \Sigma\})$ to the ordered pair $[\mu, \Delta]$ in $\Re^{2n} \times \Re^{2n^2+n}$. Associated with each set of parameters $z = \left(z^1, z^2, \ldots, z^{2n}\right)$ is a mean, $\mu(z)$, and population covariance matrix $\Sigma(z)$ that are assumed to vary smoothly with respect to z.

We may define a composite smooth function $\psi = \phi \cdot Z_c : M \to \mathcal{S}$ by

$$\psi(y) = p(x; \{\mu(Z_c(y)), \Sigma(Z_c(y))\}) \tag{7}$$

The function ψ, therefore, assigns to each set of parameters y the normal distribution function such that the mean and covariance matrix are associated with y, both of which may be estimated by experimental data. Assuming that the function ψ is regular (i.e. the differential $\phi_* \cdot Z_{c*}$ of the composite map, $\psi = \phi \cdot Z_c$, has maximal rank of four in this case), the image $D = \psi(M)$ of M in $\mathcal{S}$ is a (possibly immersed) submanifold of $\mathcal{S}$. As such, it locally satisfies the definition of a statistical manifold [1,3]. Note that it follows from basic differential geometry that if the function $y \mapsto \mu(Z_c(y))$ is regular, then ψ will also be regular. Likewise, if μ is one-to-one, then ψ will also be one-to-one, and D will be an embedded manifold and not immersed. The fact that the manifold actually has a complex structure may have interesting implications. Although this additional structure is currently being investigated, we are able to carry out the present analysis without considering it.

2.3 Model, physical, and experimental Riemannian metrics

Since D is locally a statistical manifold, the Fisher information matrix provides a natural Riemannian metric on the manifold D. Although the Fisher metric is generally positive semidefinite, it will be assumed to be positive definite. In general, a Riemannian metric provides, among other things, a way to measure the lengths of tangent vectors in D and, hence, distances within the manifold by taking infima of lengths, measured with the Riemannian metric, of curves joining pairs of points.

Therefore, the Riemannian metric is a kind of "infinitesimal" measure of distance within D. From a statistical standpoint, the Fisher metric has a particularly nice interpretation: the ability to accurately estimate a parameter μ is indicated by a Fisher metric that is "large" in terms of the parameters [3].

The differential ψ_*, represented by the Jacobian matrix with respect to the coordinate bases, carries the coordinate basis vectors $\frac{\partial}{\partial\alpha}$, $\frac{\partial}{\partial R_b}$, $\frac{\partial}{\partial C_m}$, $\frac{\partial}{\partial R_m}$ to tangent vectors in the manifold D. The Fisher metric may then be used to measure the lengths of these vectors and give a measure of the sensitivity of α, R_b, C_m, and R_m, respectively, to noise (greater length means higher sensitivity). Moreover, the sensitivity of any combination of r of these parameters may be measured as the r-dimensional volume with respect to the Fisher metric of the paralellopiped spanned by the images of those vectors. This quantity, in turn, may be computed as a certain determinant, as will be described later.

Since we are assuming regularity of ψ, we may "pullback" the Fisher metric to the manifold M. This changes the geometry of M from Euclidean to a more general Riemannian geometry that may be used independent of D to measure parameter sensitivity. By definition of the pullback metric, however, the value of the sensitivity will be the same regardless of whether it is measured in D or M. Note that one may pullback the Fisher metric even if the mapping ψ is not one-to-one; this process will remove any self-intersections that the image $\psi(M)$ may have as an immersed submanifold of D (see [7,32] for specific theorems).

The Fisher metric may be defined on the $2n$-dimensional submanifold $\phi(Z)$ of the $2n + 2n^2 + n$-dimensional space S. Hence, for $1 \leq a, b \leq 2n$ let the Fisher metric be defined as

$$g_{ab}(\theta) = E\left[\frac{\partial}{\partial\theta^a}\ln p(x;\theta)\frac{\partial}{\partial\theta^b}\ln p(x;\theta)\right], \tag{8}$$

where E represents the expectation value. The space D is at most four dimensions and inherits this metric. If the noise can be approximated as a multivariate normal distribution, then, in the absence of systematic errors $\mu(z) = \{\mu^1, \ldots, \mu^{2n}\} = \{z^1, \ldots, z^{2n}\}$ and let $\Sigma(z)$ be the covariance matrix determined by the instrumental data acquisition settings. Hence,

$$g_{ab}(z) = \frac{\partial\mu}{\partial z^a}\Sigma^{-1}\frac{\partial\mu}{\partial z^b} + \frac{1}{2}\mathrm{tr}\left(\Sigma^{-1}\frac{\partial\Sigma}{\partial z^a}\Sigma^{-1}\frac{\partial\Sigma}{\partial z^b}\right), \tag{9}$$

$$\frac{\partial\mu}{\partial z^a} = \left\{\frac{\partial\mu^1}{\partial z^a}, \frac{\partial\mu^2}{\partial z^a}, \ldots, \frac{\partial\mu^{2n}}{\partial z^a}\right\}, \tag{10}$$

and

$$\frac{\partial\Sigma}{\partial z^a} = \begin{bmatrix} \frac{\partial\Sigma^{1,1}}{\partial z^a} & \frac{\partial\Sigma^{1,2}}{\partial z^a} & \cdots & \frac{\partial\Sigma^{1,2n}}{\partial z^a} \\ \frac{\partial\Sigma^{2,1}}{\partial z^a} & \frac{\partial\Sigma^{2,2}}{\partial z^a} & \cdots & \frac{\partial\Sigma^{1,2n}}{\partial z^a} \\ \vdots & \vdots & \ddots & \\ \frac{\partial\Sigma^{2n,1}}{\partial z^a} & \frac{\partial\Sigma^{2n,2}}{\partial z^a} & \cdots & \frac{\partial\Sigma^{2n,2n}}{\partial z^a} \end{bmatrix}. \tag{11}$$

In the present study, we assume that the covariance matrix Σ varies negligibly with respect to small changes in the data state, therefore, the Fisher metric reduces to

$$g_{ab} = \frac{\partial \mu}{\partial z^a} \Sigma^{-1} \frac{\partial \mu}{\partial z^b} = \Sigma_{ab}^{-1}. \tag{12}$$

For the purposes of a sensitivity analysis, data space lengths are defined relative to instrumental noise fluctuations using the Fisher information metric. Intuitively, data space paths associated with large noise fluctuations should represent shorter effective distances than comparable paths associated with small noise fluctuations. If the noise distribution covariance varies negligibly over the range of impedance measurements and the noise at different frequencies is assumed uncorrelated, then

$$g_{ab} = \begin{bmatrix} \Sigma_{f_1}^{-1} & 0 & 0 \\ 0 & \ddots & 0 \\ 0 & 0 & \Sigma_{f_n}^{-1} \end{bmatrix}, \tag{13}$$

where

$$\Sigma_{f_k} = \begin{bmatrix} \sigma_{f_k}^{\Re\Re} & \sigma_{f_k}^{\Re\Im} \\ \sigma_{f_k}^{\Im\Re} & \sigma_{f_k}^{\Im\Im} \end{bmatrix} \tag{14}$$

represents the population variance–covariance matrix, Σ_{f_k}, at frequency f_k with real–real, real–imaginary, and imaginary–imaginary variances $\sigma_{f_k}^{\Re\Re}$, $\sigma_{f_k}^{\Im\Re}$, $\sigma_{f_k}^{\Re\Im}$, and $\sigma_{f_k}^{\Im\Im}$, respectively [16].

It is worth noting that when we assume that the noise at different frequencies is uncorrelated, we are in effect reducing the form of the Riemannian metric to that of a Riemannian product metric—in this case, the product of n 2-dimensional manifolds each having $\Sigma_{f_k}^{-1}$ as its Riemannian metric. The geometry of such a manifold generally may be derived from that of its factor manifolds. If the noise at different frequencies is correlated, then such a simple block form will not be valid. If significant local variation of Σ with respect to the parameter y is observed, then Eq. 11 must be included in Eq. 9. The corresponding second order contravariant metric tensor is

$$g^{ab} = g_{ab}^{-1} = \begin{bmatrix} \Sigma_{f_1} & 0 & 0 \\ 0 & \ddots & 0 \\ 0 & 0 & \Sigma_{f_n} \end{bmatrix}. \tag{15}$$

The data space variance–covariance matrix is also assumed to be positive definite at each frequency.

2.4 The push forward and pullback maps

The differential ψ_* can be evaluated by computing the composite map differentials ϕ_* and Z_{c*}. In this study, ϕ_* has a particularly simple form, since $\mu(z)$ is the identity map

and $\Sigma(z)$ is constant. If $Z_c(y) = z = \{z^1, z^2, \ldots, z^{2n}\}$, where the z^i represent the real and imaginary impedance components at each of the n frequencies with respect to $y = (\alpha, R_b, R_m, C_m)$, then

$$Z_{c*}(y) = \begin{bmatrix} \frac{\partial z^1}{\partial \alpha} & \frac{\partial z^1}{\partial R_b} & \frac{\partial z^1}{\partial C_m} & \frac{\partial z^1}{\partial R_m} \\ \frac{\partial z^2}{\partial \alpha} & \frac{\partial z^2}{\partial R_b} & \frac{\partial z^2}{\partial C_m} & \frac{\partial z^2}{\partial R_m} \\ \vdots & \vdots & \vdots & \vdots \\ \frac{\partial z^{2n}}{\partial \alpha} & \frac{\partial z^{2n}}{\partial R_b} & \frac{\partial z^{2n}}{\partial C_m} & \frac{\partial z^{2n}}{\partial R_m} \end{bmatrix}. \tag{16}$$

The dual, or transpose, is defined as

$$Z_c^*(z) = \begin{bmatrix} \frac{\partial z^1}{\partial \alpha} & \frac{\partial z^2}{\partial \alpha} & \cdots & \frac{\partial z^{2n}}{\partial \alpha} \\ \frac{\partial z^1}{\partial R_b} & \frac{\partial z^2}{\partial R_b} & \cdots & \frac{\partial z^{2n}}{\partial R_b} \\ \frac{\partial z^1}{\partial C_m} & \frac{\partial z^2}{\partial C_m} & \cdots & \frac{\partial z^{2n}}{\partial C_m} \\ \frac{\partial z^1}{\partial R_m} & \frac{\partial z^2}{\partial R_m} & \cdots & \frac{\partial z^{2n}}{\partial R_m} \end{bmatrix}. \tag{17}$$

The measurement map $\phi : Z \to \mathcal{S}$ is assumed to be of the form $\mu = z$, and Σ is set by the instrumentation settings. This form of analysis plays an important role in the evaluation of a model cellular impedance function and its suitability for numerical parameter optimization.

2.5 Parameter precision analysis

We will denote coordinate basis vectors in M by $\frac{\partial}{\partial y^a}$. If g denotes, as above, the Fisher metric in D, then the pullback metric is

$$G(y) = Z_c^* g\left(\frac{\partial}{\partial y^a}, \frac{\partial}{\partial y^b}\right) = g\left(Z_{c*}\frac{\partial}{\partial y^a}, Z_{c*}\frac{\partial}{\partial y^b}\right), \tag{18}$$

where $\partial/\partial y^a$, allows a state dependent model space sensitivity analysis to be carried out. The model state space dependent sensitivity for each parameter can, therefore, be defined as the length of each coordinate basis, or parameter, vector $\partial/\partial y^a$ under this metric. An additional sensitivity analysis can also be defined for various combinations of these parameter vectors. Two parameter vectors define an area, three a volume, and so forth. The following determinant components, derived from the metric, define the sensitivity associated with different combinations of parameters:

$$\begin{aligned} \Lambda^1_\alpha &= \sqrt{\det(G_{\alpha\alpha})} & \Lambda^1_{R_b} &= \sqrt{\det(G_{R_b R_b})} \\ \Lambda^1_{C_m} &= \sqrt{\det(G_{C_m C_m})} & \Lambda^1_{R_m} &= \sqrt{\det(G_{R_m R_m})} \end{aligned} \tag{19}$$

$$\Lambda^2_{\alpha R_b} = \sqrt{\det\begin{pmatrix} G_{\alpha\alpha} & G_{\alpha R_b} \\ G_{R_b\alpha} & G_{R_b R_b} \end{pmatrix}} \quad \Lambda^2_{\alpha C_m} = \sqrt{\det\begin{pmatrix} G_{\alpha\alpha} & G_{\alpha C_m} \\ G_{C_m\alpha} & G_{C_m C_m} \end{pmatrix}}$$

$$\Lambda^2_{\alpha R_m} = \sqrt{\det\begin{pmatrix} G_{\alpha\alpha} & G_{\alpha R_m} \\ G_{R_m\alpha} & G_{R_m R_m} \end{pmatrix}} \quad \Lambda^2_{R_b R_b} = \sqrt{\det\begin{pmatrix} G_{R_b R_b} & G_{R_b C_m} \\ G_{C_m R_b} & G_{C_m C_m} \end{pmatrix}}$$

$$\Lambda^2_{R_b R_m} = \sqrt{\det\begin{pmatrix} G_{R_b R_b} & G_{R_b R_m} \\ G_{R_m R_b} & G_{R_m R_m} \end{pmatrix}} \quad \Lambda^2_{C_m C_m} = \sqrt{\det\begin{pmatrix} G_{C_m C_m} & G_{C_m R_m} \\ G_{R_m C_m} & G_{R_m R_m} \end{pmatrix}} \tag{20}$$

$$\Lambda^3_{\alpha R_b C_m} = \sqrt{\det\begin{pmatrix} G_{\alpha\alpha} & G_{\alpha R_b} & G_{\alpha C_m} \\ G_{R_b\alpha} & G_{R_b R_b} & G_{R_b C_m} \\ G_{C_m\alpha} & G_{C_m R_b} & G_{C_m C_m} \end{pmatrix}}$$

$$\Lambda^3_{\alpha R_b R_m} = \sqrt{\det\begin{pmatrix} G_{\alpha\alpha} & G_{\alpha R_b} & G_{\alpha R_m} \\ G_{R_b\alpha} & G_{R_b R_b} & G_{R_b R_m} \\ G_{R_m\alpha} & G_{R_m R_b} & G_{C_m R_m} \end{pmatrix}}$$

$$\Lambda^3_{\alpha C_m R_m} = \sqrt{\det\begin{pmatrix} G_{\alpha\alpha} & G_{\alpha C_m} & G_{\alpha R_m} \\ G_{C_m\alpha} & G_{C_m C_m} & G_{C_m R_m} \\ G_{R_m\alpha} & G_{R_m C_m} & G_{R_m R_m} \end{pmatrix}}$$

$$\Lambda^3_{R_b C_m R_m} = \sqrt{\det\begin{pmatrix} G_{R_b R_b} & G_{R_b C_m} & G_{R_b R_m} \\ G_{C_m R_b} & G_{C_m C_m} & G_{C_m R_m} \\ G_{R_m R_b} & G_{R_m C_m} & G_{R_m R_m} \end{pmatrix}} \tag{21}$$

$$\Lambda^4_{\alpha R_b C_m R_m} = \sqrt{\det\begin{pmatrix} G_{\alpha\alpha} & G_{\alpha R_b} & G_{\alpha C_m} & G_{\alpha R_m} \\ G_{R_b\alpha} & G_{R_b R_b} & G_{R_b C_m} & G_{R_b R_m} \\ G_{C_m\alpha} & G_{C_m R_b} & G_{C_m C_m} & G_{C_m R_m} \\ G_{R_m\alpha} & G_{R_m R_b} & G_{R_m C_m} & G_{R_m R_m} \end{pmatrix}} \tag{22}$$

The determinant components produced by the metric $Z_c^* g$ provide a basis for a model space sensitivity given each possible combination of parameters. Sections of these determinant components were examined over the set of model states ($0.001\ \Omega^{0.5}\ \text{cm} < \alpha < 10\ \Omega^{0.5}\ \text{cm}$) $\times$ ($0.001\ \Omega\ \text{cm}^2 < R_b < 10\ \Omega\ \text{cm}^2$) $\times$ ($0.01\ \mu\text{F}\,\text{cm}^{-2} < C_m < 100\ \mu\text{F}\,\text{cm}^{-2}$) $\times$ ($1\ \Omega\,\text{cm}^2 < R_m < 10\ \text{k}\Omega\,\text{cm}^2$).

We conclude this section with some comments about our two most basic assumptions: the regularity of the map ψ and the positive semidefinite assumption of the Fisher information metric. If the mapping ψ is not regular, then, although one can formally discuss the pullback, it will not be positive definite and, hence, not a Riemannian metric. One could still compute Eqs. 19–22 using Eq. 18. However, if ψ is not regular, then the vectors $Z_{c^*}\left(\frac{\partial}{\partial y^a}\right)$ are linearly dependent and $\Lambda^4 = 0$. Model states where ψ is not regular indicate that the mapping ψ will introduce parameter identifiability

problems or an inability to separately resolve the parameter set. On the other hand, if the Fisher metric is not positive definite, then we would also have $\Lambda^4 = 0$. This follows from basic linear algebra and the fact that the Fisher metric is always positive semi-definite. In this case, the data sample probability distribution will introduce parameter identifiability problems. A reasonable approach then is to collect data to compute Λ^4; as long as Λ^4 is non-zero then these two basic assumptions are satisfied at least for nearby data points. If Λ^4 is non-zero for a fairly large data set, then it is reasonable to assume that ψ is regular and the Fisher metric is positive definite at all points. If Λ^4 is singular, specific parameter subsets can be tested by examining the determinant components given by Eqs. 19–21. The regularity of ψ and the parameter precision will also depend on the choice of sampled frequencies. For example, using a single frequency will always result in non-regularity for basic reasons of dimensionality. If non-regularity is observed experimentally, collecting data at different or additional frequencies may resolve the problem.

3 Methods and materials

3.1 Cell culture

Porcine endothelial cells were isolated from fresh pulmonary arteries obtained from a local abattoir. Endothelial cells between passages four and eight were used for this study. Cultures were identified as endothelial cells by their characteristic uniform morphology, uptake of acetylated LDL, and by indirect immunofluorescent staining for Factor VIII. Five well gold electrodes, purchased from Applied Biophysics (Troy NY), were coated with fibronectin (BD Biosciences) using a 100 μg mL^{-1} solution. Endothelial cells, grown to confluence in a 100 mm culture dish, were trypsinized using 0.05% trypsin (GibcoBRL). The cells were then spun down, the trypsin drawn off, and then re-suspended in 10 mL M199. From this cell solution, 400 μL were added to the electrode wells maintaining a seeding density of approximately 10^5 cells cm^{-2}. Endothelial cells were permitted to attach for 16 h in an incubator. The entire surface of each well was carefully examined for endothelial cell confluence and cobblestone morphology.

3.2 Experimental estimation of data sub-space and metric

Figure 2 shows a schematic illustration of the impedance measuring system. A lock-in amplifier (Stanford Research SR830) provided 1V AC reference signals between 10 Hz and 100 kHz to an electrode via a 1 MΩ resistor. The sampling frequency was set to 32 Hz, and a total of 512 samples were made over a 16-second time period. The filter time constant was set to 30 ms, and the filter roll off was set to 12 dB/decade. Synchronization filtering ensured that harmonic noise below 200 Hz did not corrupt the voltage measurements. The measured voltages were converted to corresponding impedance values based on the circuit model shown in Fig. 2.

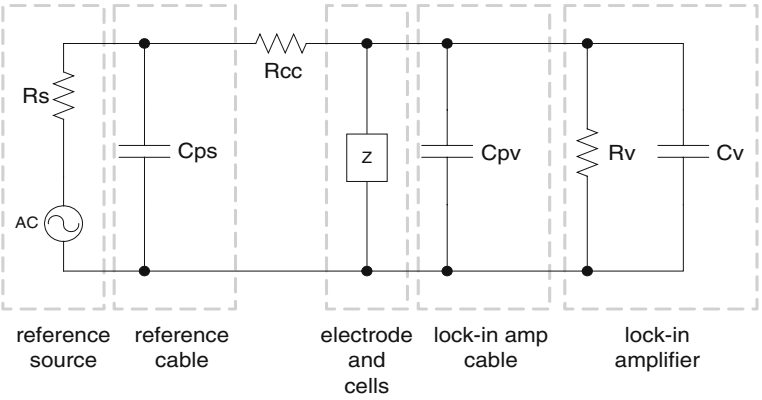

Fig. 2 Cellular impedance measuring circuit configuration. The ac generator provides a 1V signal via a 1 MΩ resistor, Rcc. The source resistance, Rs, was 50 Ω, and the phase sensitive detector had an input impedance equivalent to a parallel resistor and capacitor, Rv and Cv, combination equal to 10 MΩ and 25 pF, respectively. The measured values of the coaxial lead parasitic elements Cps and Cpv were approximately 86 pF each. The detected voltage was converted into an equivalent impedance based on this circuit configuration

Unbiased estimates of the impedance averages were obtained from the N data samples at each frequency using the relation

$$\overline{x^{f_k}} = \frac{1}{N}\sum_{i=1}^{N} x_i^{f_k}. \tag{23}$$

Unbiased estimates of the data variance–covariance matrix at each frequency,

$$S_{f_k} = \begin{bmatrix} s_{f_k}^{\Re\Re} & s_{f_k}^{\Re\Im} \\ s_{f_k}^{\Im\Re} & s_{f_k}^{\Im\Im} \end{bmatrix}, \tag{24}$$

were obtained from data measurements using the relations

$$\begin{aligned}
s_{f_k}^{\Re\Re} &= \sum_{i=1}^{N} \frac{\left(x_i^{\Re f_k} - \overline{x^{\Re f_k}}\right)\left(x_i^{\Re f_k} - \overline{x^{\Re f_k}}\right)}{(N-1)}, \\
s_{f_k}^{\Re\Im} &= \sum_{i=1}^{N} \frac{\left(x_i^{\Re f_k} - \overline{x^{\Re f_k}}\right)\left(x_i^{\Im f_k} - \overline{x^{\Im f_k}}\right)}{(N-1)}, \\
s_{f_k}^{\Im\Re} &= \sum_{i=1}^{N} \frac{\left(x_i^{\Im f_k} - \overline{x^{\Im f_k}}\right)\left(x_i^{\Re f_k} - \overline{x^{\Re f_k}}\right)}{(N-1)}, \quad \text{and} \\
s_{f_k}^{\Im\Im} &= \sum_{i=1}^{N} \frac{\left(x_i^{\Im f_k} - \overline{x^{\Im f_k}}\right)\left(x_i^{\Im f_k} - \overline{x^{\Im f_k}}\right)}{(N-1)}.
\end{aligned} \tag{25}$$

The standard deviations of the real and imaginary impedance components follow from

$$s_{f_k}^{\Re} = \sqrt{s_{f_k}^{\Re\Re}} \quad \text{and} \quad s_{f_k}^{\Im} = \sqrt{s_{f_k}^{\Im\Im}}, \tag{26}$$

respectively. The real and imaginary impedance correlation coefficient can be calculated using the relation

$$r_{f_k}^{\Re\Im} = r_{f_k}^{\Im\Re} = \frac{s_{f_k}^{\Re\Im}}{\sqrt{s_{f_k}^{\Re\Re}}\sqrt{s_{f_k}^{\Im\Im}}}. \tag{27}$$

The unbiased variance–covariance matrix, S_{f_k}, at each frequency sample point, f_k, provides an unbiased estimate of the population variance–covariance matrix Σ_{f_k}.

4 Results

Model states consistent with experimental estimates of the average frequency dependent impedances define the appropriate domain of model states, and noise fluctuation measurements provide an estimate of the Fisher metric. Once the model state domain and Fisher metric are defined, the sensitivity of the function mapping each of these states into the data space can be evaluated. The square root of the data space metric determinant components pulled back to the model space quantify the model state dependent sensitivity and stability of the different parameter combinations.

4.1 Experimental estimates of the data space submanifold and tangent bundle metric

Figure 3 summarizes the statistics of a series of experimentally acquired frequency dependent naked and cell covered electrode impedance measurements. At each frequency, the mean and variance of 512 data points sampled at a rate of 32 Hz over a 16 second time interval produced a similar pattern among five different samples. As the top two figures indicate, the real and imaginary impedance fluctuations exhibit an overall decrease with increasing frequency. The average of the real and imaginary components also decrease with increasing frequency. The optimized fit to the mean cell covered electrode data gives the parameter values $\alpha = 4.895 \pm 0.003\ \Omega^{0.5}$ cm, $R_b = 3.866 \pm 0.004\ \Omega\ \text{cm}^2$, $C_m = 1.4534 \pm 0.0005\ \mu\text{F cm}^{-2}$, and $R_m = 3.447 \pm 0.005\ \text{k}\Omega\ \text{cm}^2$. The correlation coefficients are $\alpha - R_b = -0.9902$, $\alpha - C_m = -0.9067$, $\alpha - R_m = -0.9249$, $R_b - C_m = 0.9389$, $R_b - R_m = 0.9487$, and $C_m - R_m = 0.9164$. Error and correlation coefficients are based on the χ^2 curvature at the optimized minimum point [25].

4.2 Data space parameter sensitivity analysis

Figure 4 illustrates the results of a sensitivity analysis using the data space metric to evaluate the length of the vector components, $Z_{c*}(y)\partial/\partial y^a$, at the point ($\alpha = 4.895\ \Omega^{0.5}$ cm, $R_b = 3.866\ \Omega\ \text{cm}^2$, $C_m = 1.4534\ \mu\text{F cm}^{-2}$, $R_m = 3.447\ \text{k}\Omega\ \text{cm}^2$).

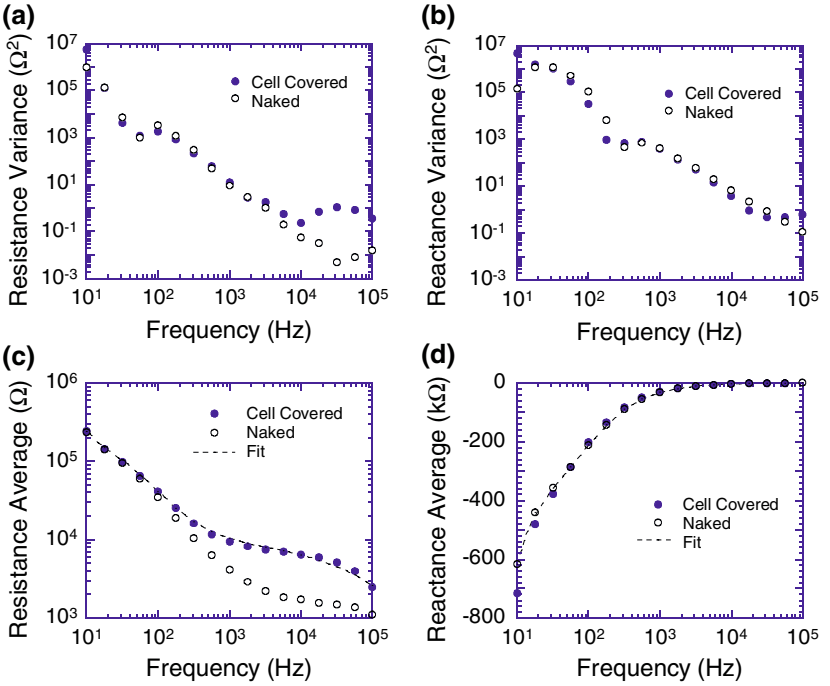

Fig. 3 Representative frequency dependent statistical summary of experimentally acquired naked electrode impedances and cell covered electrode impedances following sixteen hours of attachment: **a** resistance variance, **b** reactance variance, **c** mean resistance, and **d** mean reactance. Naked electrode variance estimates define the metric. The optimized fit to the mean cell covered electrode data gives the parameter values: $\alpha = 4.895 \pm 0.003\ \Omega^{0.5}$ cm, $R_b = 3.866 \pm 0.004\ \Omega\,\text{cm}^2$, $C_m = 1.4534 \pm 0.0005\ \mu\text{F}\,\text{cm}^{-2}$, and $R_m = 3.447 \pm 0.005\,\text{k}\Omega\,\text{cm}^2$. The correlation coefficients are $\alpha - R_b = -0.9902$, $\alpha - C_m = -0.9067$, $\alpha - R_m = -0.9249$, $R_b - C_m = 0.9389$, $R_b - R_m = 0.9487$, and $C_m - R_m = 0.9164$. Error and correlation coefficients are based on the χ^2 curvature at the optimized minimum point

The metric in this case was evaluated using Eq. 13 and the unbiased estimators given by Eq. 25. Each set of real and imaginary points represents the length of the data space vector components $Z_{c*}(y)\partial/\partial y^a$ under the metric $g_{ab}(z = Z_c(y))$, where each component a or b represents a frequency and real or imaginary part. At this point, changes in R_m, i.e., $\partial/\partial R_m$, show the least sensitivity, which is consistent with the very large errors associated with this parameter. Only over the narrow range of R_m values between 10 and 1 kΩ is there any appreciable sensitivity in the parameter R_m. Between parameter values of 10 and 100 Ω cm, the sensitivity reaches a maximum. Outside of this range, the impedance sensitivity to R_m is negligible. The parameter C_m shows the greatest sensitivity at higher frequencies.

4.3 Model to data space cellular impedance mapping Z_c

Figure 5 shows the normalized changes in resistance and reactance as a function of time during an endothelial cell attachment based on experimental measurements. With

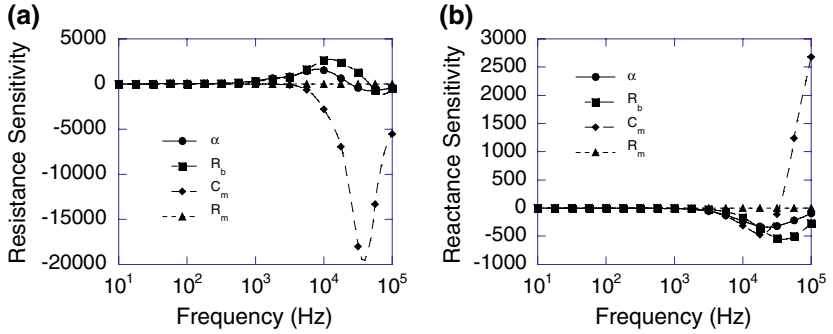

Fig. 4 Data space sensitivity analysis at the model space point $y = \{\alpha = 4.895\ \Omega^{0.5}\ \text{cm}, R_b = 3.866\ \Omega\ \text{cm}^2, C_m = 1.4534\ \mu\text{F cm}^{-2}, R_m = 3.447\ \text{k}\Omega\ \text{cm}^2\}$, corresponding to the estimated parameters found analyzing the data shown in Fig. 3. Each point represents the length of the vector $Z_{c*}(y)\partial/\partial y^a$ component in the physical space coordinate basis $\partial/\partial z^a$ under the metric $g_{ab}(x)$, where $z = Z_c(y)$. **a** The n real components to the sensitivity analysis are most sensitive between 1 and 100 kHz. **b** The n imaginary components to the sensitivity analysis indicate that the parameter C_m becomes increasingly sensitive at higher frequencies. Both the real and imaginary parts indicate that the $Z_{c*}(y)\partial/\partial R_m$ components are relatively insensitive to changes in the parameter $\partial/\partial R_m$ for the noise distribution that g_{ab} represents

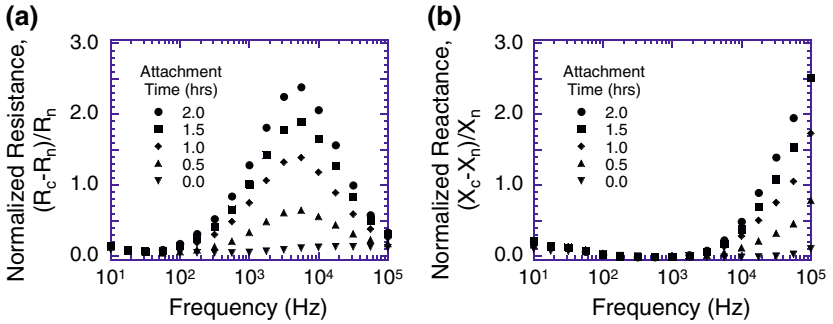

Fig. 5 Time dependent normalized impedance changes. **a** Cell covered electrode resistance normalized to the naked electrode resistance, $(R_c - R_n)/R_n$, as a function of frequency and time following inoculation. **b** Cell covered reactance normalized to the naked electrode reactance, $(X_c - X_n)/X_n$, as a function of frequency and time following inoculation. As endothelial cells form a monolayer on the electrode surface, the normalized resistance and reactance increase during the attachment process

increasing time, the normalized resistance and reactance increase. Figure 6 shows a model simulation with the parameters $\alpha = 4.895\ \Omega^{0.5}$ cm, $R_b = 3.866\ \Omega\,\text{cm}^2$, $C_m = 1.4534\,\mu\text{F cm}^{-2}$, and $R_m = 3.445\,\text{k}\Omega\,\text{cm}^2$. For clarity and comparison with previously published work, the mappings are expressed as normalized curves [14]. The results of these simulations allow us to set the reasonable parameter domain $(0.001\ \Omega^{0.5}\ \text{cm} < \alpha < 10\ \Omega^{0.5}\ \text{cm}) \times (0.001\ \Omega\ \text{cm}^2 < R_b < 10\ \Omega\ \text{cm}^2) \times (0.01\ \mu\text{F cm}^{-2} < C_m < 100\ \mu\text{F cm}^{-2}) \times (1\ \Omega\ \text{cm}^2 < R_m < 10\ \text{k}\Omega\ \text{cm}^2)$. The shapes of these plots are very similar. From this data it is also apparent that much larger changes in R_m are required to produce similar changes in α and R_b.

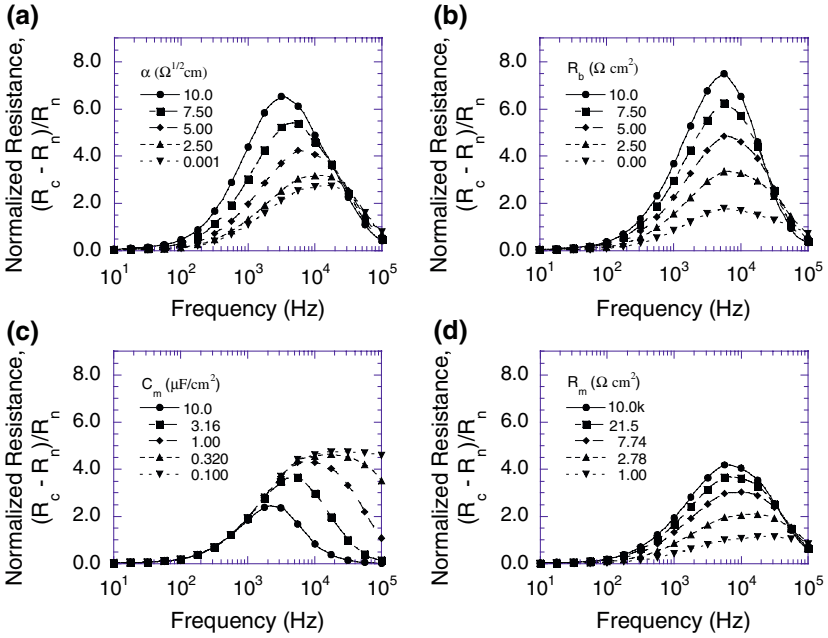

Fig. 6 Simulated normalized resistances as a function of frequency and changes in **a** α, **b** R_b, **c** C_m, and **d** R_m. The normalized resistance is defined as $(R_c - R_n)/R_n$, where R_c is the cell covered resistance and R_n is the naked electrode resistance. For each set of simulations, three of the set of four parameters were fixed, and the remaining parameter was varied as indicated in the legend. The fixed simulation parameters were $\alpha = 4.895\ \Omega^{0.5}$ cm, $R_b = 3.866\ \Omega\,\text{cm}^2$, $C_m = 1.4534\ \mu\text{F cm}^{-2}$, and $R_m = 3.447\ \text{k}\Omega\,\text{cm}^2$. This range of parameters produce impedances in qualitative agreement with the experimentally measured cell covered electrode values. Increasing R_m above 20 $\Omega\,\text{cm}^2$ produces only a small increase in the normalized resistance

4.4 Model space parameter precision analysis

Figure 7 shows the model state dependent parameter sensitivity, considering each parameter separately. The length of each contravariant parameter vector was evaluated using the pullback of the data space metric. The parameters C_m and R_m were fixed to $1.4534\ \mu\text{F cm}^{-2}$ and $3.447\ \text{k}\Omega\,\text{cm}^2$, respectively. The parameter α becomes relatively insensitive as R_b approaches zero. The sensitivity of the parameter R_b monotonically decreases with increasing α and R_b model states. Model states with decreasing values of both α and R_b are also associated with decreasing sensitivities of both C_m and R_m. Note also that the parameter R_m is relatively insensitive over the range of model states illustrated here. Repeating this analysis with increasing values of C_m systematically decreased the sensitivity of the remaining three parameters. Similarly, model states with decreasing values of R_m were associated with both decreasing sensitivities of the remaining three parameters and increasing sensitivity of R_m itself.

Figure 8 summarizes the stability of the parameter pairs using the area defined by the parameter basis vectors. The square root of the 2×2 data space metric pullback determinant components quantify these areas in terms of the instrumental noise levels.

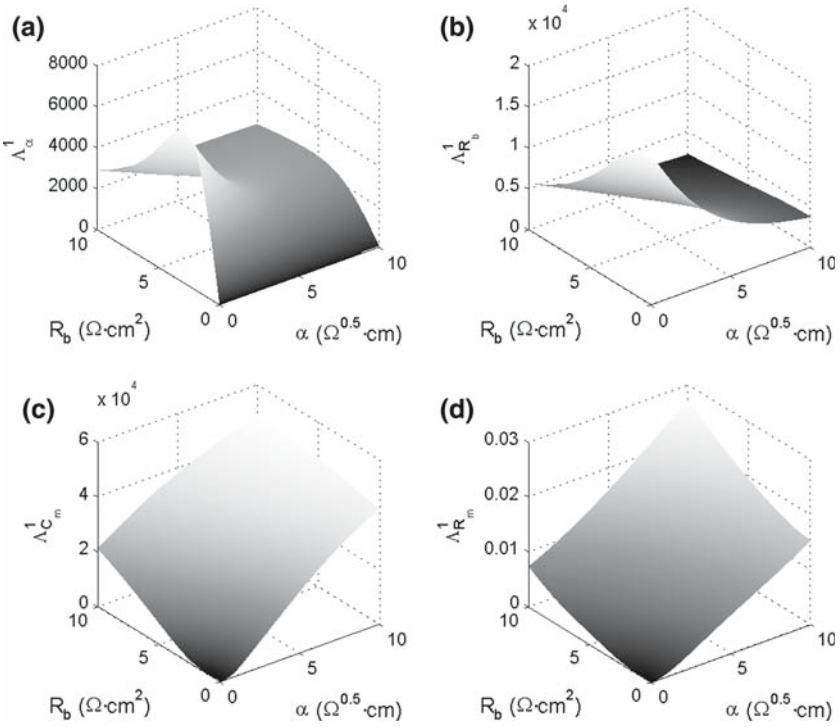

Fig. 7 Model state dependent contravariant parameter vector lengths, $\partial/\partial y^a$, evaluated using the data space metric pullback $Z_c^* g_{ab}(Z_c(y))$. None of the parameter vector lengths go to zero at any point over the model state domain. The parameters C_m and R_m were fixed to 1.4534 μF cm^{-2} and 3.447 kΩ cm^2, respectively. **a** The length of the vector $\partial/\partial\alpha$ approaches unity over model states associated with small values of R_b. **b** The vector $\partial/\partial R_b$ is stable over the entire model domain considered here. **c** The length of the membrane capacitive component $\partial/\partial C_m$ approaches unity only over a very small neighborhood near the point where $\alpha \to 0$ and $R_b \to 0$. **d** The length of $\partial/\partial R_m$ is less than unity over the entire model state domain and is therefore unstable. Model states associated decreasing values of R_m, however, produce increasing sensitivity, or length, of $\partial/\partial R_m$

The parameters C_m and R_m were fixed to 1.4534 μF cm^{-2} and 3.447 kΩ cm^2 and the model states on the $\alpha - R_b$ plane shown. In all cases, model states with small values of α and R_b are relatively insensitive when the two parameters are considered together. Repeating these calculations with either increasing C_m or R_m model states produces a systematic decrease in the section values. Parameter pairs that include R_m have clearly defined regions of instability, where the area becomes less than unity.

Figure 9 shows the volume spanned by combinations of three contravariant parameter vectors under the data space metric. The square root of the 3×3 determinant components derived from the data space metric pullback quantifies the volume in terms of the instrumental noise levels. In all cases, small values of R_b produce relatively less stable values. Model states associated with small values of α and R_b and large values of C_m and R_m produce insensitive values for all sets of three parameters.

Figure 10 shows the hyper volume spanned by all four parameters when evaluated using the data space metric pullback. The square root of the 4×4 data space metric

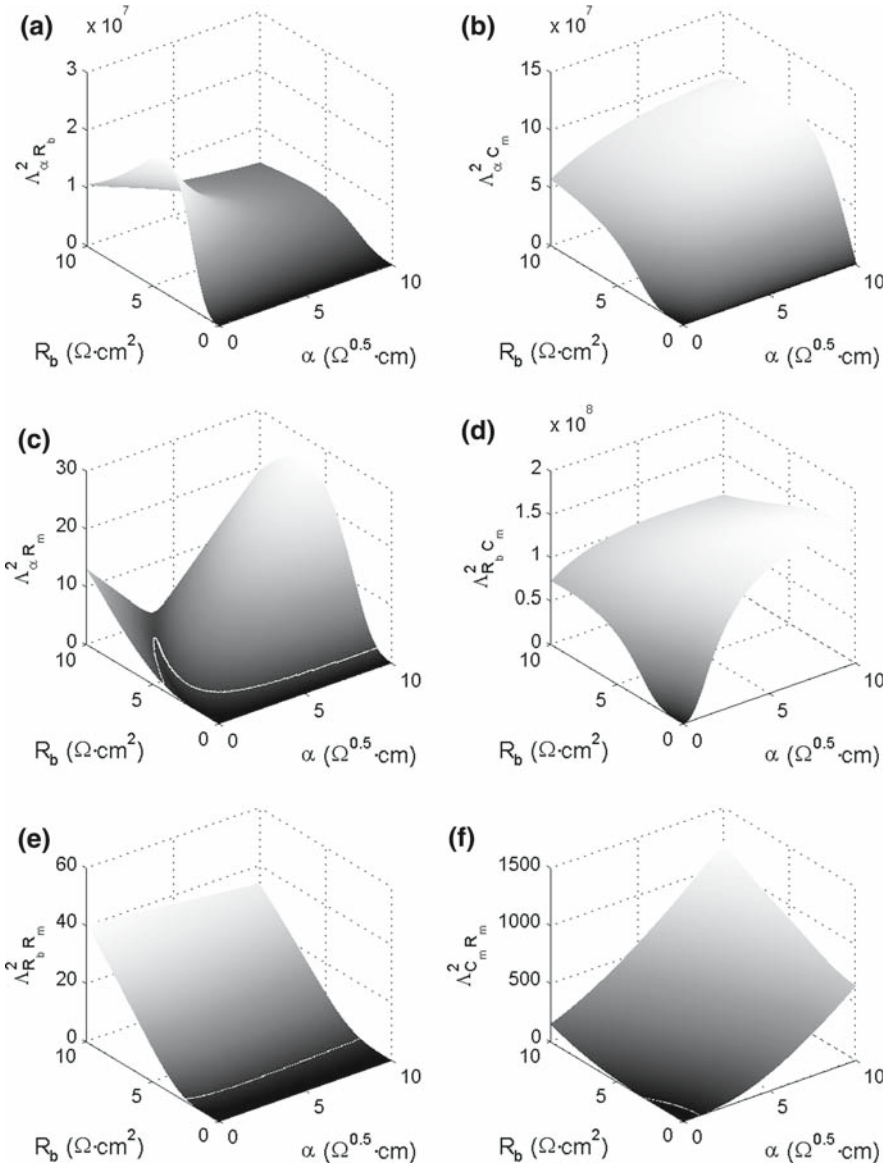

Fig. 8 Model state dependent areas defined by pairs of contravariant parameter vectors, $\partial/\partial X^A$, evaluated using the data space metric pullback $Z_c^* g_{ab}(Z_c(y))$. Areas defined by pairs of contravariant parameter vectors follow from the 2×2 data metric determinant components: **a** $\Lambda^2_{\alpha R_b}$, **b** $\Lambda^2_{\alpha C_m}$, **c** $\Lambda^2_{\alpha R_m}$, **d** $\Lambda^2_{R_b C_m}$, **e** $\Lambda^2_{R_b R_m}$, and **f** $\Lambda^2_{C_m R_m}$. Transition regions where the areas become equal to unity are indicated by lines. The parameters C_m and R_m were fixed to 1.4534 μF cm^{-2} and 3.447 kΩ cm^2, respectively

determinant shows a pattern of decreasing stability with decreasing values of α and R_b. The model state values of C_m and R_m are again fixed to 1.4534 μF cm^{-2} and 3.447 kΩ cm^2, respectively. The parameter sensitivity progressively worsens as the

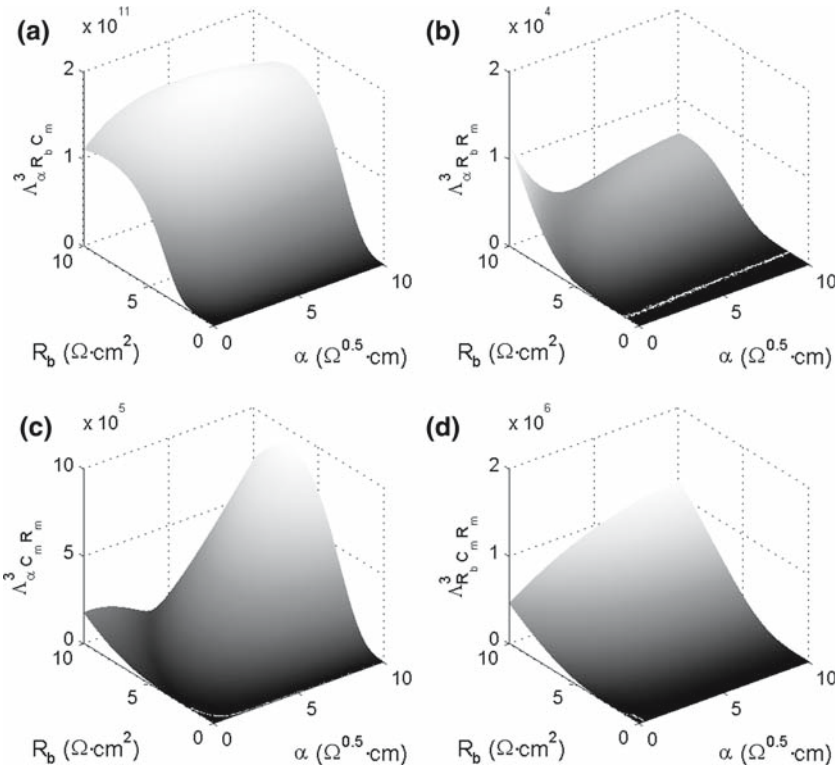

Fig. 9 Model state dependent volumes defined by triples of contravariant parameter vectors, $\partial/\partial y^a$, evaluated using the data space metric pullback $Z_c^* g_{ab}(Z_c(y))$. Volumes are defined by the 3×3 determinant components: **a** $\Lambda^3_{\alpha R_b C_m}$, **b** $\Lambda^3_{\alpha R_b R_m}$, **c** $\Lambda^3_{\alpha C_m R_m}$, and **d** $\Lambda^3_{R_b C_m R_m}$. The parameters C_m and R_m were fixed to 1.4534 μF cm^{-2} and 3.447 kΩ cm^2, respectively

value of R_m decreases. A similar degradation in the parameter sensitivity occurs with increasing values of the C_m model states.

5 Discussion

The estimation of cellular barrier function parameters using frequency dependent impedance measurements and the non-linear optimization of cellular models has a number of potential applications in biology and bioengineering [12,14]. The non-linear nature of these models and the ubiquitous presence of instrumental noise, however, complicate a precision or sensitivity analysis of these parameters. Noise levels can vary from one physical impedance state to another, and the sensitivity of the model parameters can vary from one model state to another depending on the nature of the model function. Furthermore, the choice of which parameters to fix and which to optimize can dramatically change the stability of the analysis. Geometric constructs provide a natural foundation for quantifying parameter precision with respect to a

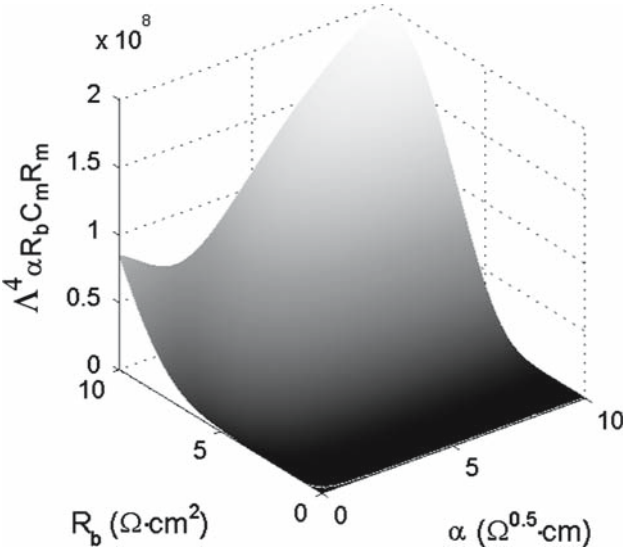

Fig. 10 The hyper volume defined by all four contravariant parameter vectors. The hyper volume follows from the 4×4 determinant component $\Lambda^4_{\alpha R_b C_m R_m}$. Model states with small values of α and R_b are associated with relatively smaller sensitivities in the four parameters. The parameters C_m and R_m were fixed to 1.4534 μF cm^{-2} and 3.447 kΩ cm^2, respectively

particular model function, instrumental noise levels, and data acquisition settings. The Fisher information metric gives a measure of distance in terms of instrumental noise levels. By pulling this metric back to an abstract model space using a model function, it is possible to set limits on the obtainable parameter precision. Furthermore, the determinant components produced by this metric provide a natural framework for a precision analysis given various parameter combinations.

The parameters under consideration and the degrees of freedom associated with data acquisition define local coordinate systems on the model and data spaces, respectively. In this study, the model space parameters represent the impedance path components through a cellular monolayer. The cellular impedance model function maps these parameters into a subset of a physical and data space of all possible experimental outcomes. Constraints based on the range of expected experimental results set bounds on the model space domain. The physical and data space coordinate system in this case is defined in terms of the n frequency dependent real and imaginary impedance values of a $2n$-dimensional space. The sampled frequencies on the physical and data space play an important role in the attainable model spatial resolution.

This study identifies a data space Riemannian metric [7], $g_{ab}(z)$, with the Fisher information matrix. An estimate of this metric can be obtained using direct experimental measurements of the impedance statistics at each frequency [16]. Since the noise variance–covariance matrix is actually the contravariant version of the covariant metric tensor, it must be non-singular to define the components of its inverse or associated covariant bilinear form $g_{ab}(z)$. In general, the pullback of contravariant

components and the push-forward of both covariant and contravariant components require regularity of the model to data space mapping.

In general, the data space metric, $g_{ab}(z)$, will be a function of the data space state defined by the real and imaginary impedance components over the n measured frequencies. This can arise, for example, when capacitively coupled deterministic noise, such as sixty Hertz noise, produces increasing noise levels with increasing load impedance values. Adequate filtering, however, can be used to significantly reduce this effect [12]. As a result, this study assumes that the cell covered electrode instrumental noise is similar to that of the naked electrode and is relatively constant over the range of cell covered impedances. Using an electrode model with calibration resistors and capacitors, the state dependent nature of the data space electrode noise can be included where necessary. This consideration becomes important when distinguishing fluctuations produced by instrumental noise and from those produced by cellular fluctuations [15].

It is also important to realize that the metric in this study is approximated using Gaussian statistics. A Gaussian approximation to the instrumental noise breaks down when filtering and non-Gaussian noise sources, such as sixty-Hertz, discretization, and harmonic noise sources are present [12]. The extension of this form of analysis to account for non-Gaussian instrumental noise may be necessary in these cases.

Ignoring the noise correlation at different frequencies requires careful justification. Since the voltage data at each frequency are not sampled simultaneously, they can be treated as independent sets of events as far as random noise is concerned. That is, assuming the low pass filter time constant is much shorter than the time interval between successive frequency measurements. The effects of deterministic noise, such as a sixty Hertz or synchronous noise, can also be ignored provided low pass filtering and time averaging are used to reduce these components to negligible values. The noise components and their reduction using filtering have been treated extensively in another study [12].

The nature of the function mapping the model space into the data space determines much of the success in optimization a given set of parameters. If the function fails to be regular over the specified model space domain, parameter identifiability problems will arise regardless of how little instrumental noise is present. Taking different combinations or fewer free parameters is a possible solution to this problem. Even if the mapping is regular, there is no guarantee that the map will be one to one over the specified model domain. When this happens, more than one set of parameters can represent the same data point.

Applying the data space metric to evaluate the length of the impedance components in the data space for a given model state quantifies which data components are most sensitive for a given level of instrumental noise. When the data space metric is applied to the submanifold tangent bundle defined by the model space map, the individual components illustrate which components are most sensitive to data changes. This can provide a guide for optimizing the data sampling and showing where the model is most sensitive to systematic errors.

Defining the model space metric tensor as the pullback of data space metric provides valuable insight into the numerical stability of the problem as a function of the model state even before any form of numerical optimization is attempted. Analyzing

the unit vectors over the model space tangent bundle using the pullback of the data space metric shows more compactly the state dependence of the parameters. The pullback of a data space metric, $Z_c^* g_{ab}(z = Z_c(y))$, gives a quantitative measure of the model space resolution. The model space metric defines the separation between model space coordinate points that can be successfully resolved using numerical optimization methods. Minimal distances defined using this metric quantify the model space resolution.

The corresponding point spread function, defined in terms of the contravariant associated tensor $G^{AB}(X)$, can also be used to define model space resolution. For a given pair of points on the model space, overlapping point spread functions, defined in terms of either $G^{AB}(X)$ or $\chi^2(y)$, are indicative of numerically un-resolvable model states. The point-spread functions are state dependent, have eigenvectors rotated with respect to the original coordinates, and eigenvalues that indicate very different degrees of resolution in the two orthogonal directions. This is essentially a globalized version of principle component, or factor, analysis.

The ability to resolve separate parameters based on a series of experimental measurements is referred to as identifiability. In non-linear optimization problems, shifts in the value of one parameter can be compensated by shifts in one or more other parameters. In extreme cases, it is not possible to separately resolve two or more parameters. Parameter identifiability is illustrated in both the data space and model space. This study illustrates identifiability in three ways. Using the forward model mapping, it is apparent that the similarity in the image sets of the impedance function is a significant indication of identifiability problems. The similarity in the shape of the tangent curves further quantifies this. On the model space, the geometry between the vectors $\partial/\partial\alpha$, $\partial/\partial R_b$, $\partial/\partial C_m$, and $\partial/\partial R_m$ illustrates state dependent identifiability. Sections of the determinant components illustrate which combinations of these vectors will produce identifiability and stability problems.

6 Conclusion

Within the numerical tolerance of this study, no singularities in any of the parameter combinations where observed over the model state domain ($0.001\ \Omega^{0.5}\ \text{cm} < \alpha < 10\ \Omega^{0.5}\ \text{cm}$) $\times$ ($0.001\ \Omega\ \text{cm}^2 < R_b < 10\ \Omega\ \text{cm}^2$) $\times$ ($0.01\ \mu\text{F cm}^{-2} < C_m < 100\ \mu\text{F cm}^{-2}$) $\times$ ($1\ \Omega\ \text{cm}^2 < R_m < 10\ \text{k}\Omega\ \text{cm}^2$). The subcellular and intercellular impedance paths, represented by parameters, exhibit a maximum sensitivity between 1 and 100 kHz for the filter settings used in this study. The model parameter C_m showed the greatest sensitivity. The parameter R_m is relativity insensitive for values exceeding $20\ \Omega\ \text{cm}^2$.

References

1. Amari, S.: Differential–Geometrical Methods of Statistics. Lecture Notes in Statistics, vol. 25. Springer, Berlin (1985)
2. Amari, S.: Fisher information under restriction of Shannon information. Ann. Inst. Statist. Math. **41**, 623–648 (1989)

3. Armari, S., Nagaoka, H.: Methods of Information Geometry. AMS and Oxford University Press, New York (2000)
4. Amari, S.: Dualistic geometry of the manifold of higher-order neurons. Neural Networks **4**, 443–451 (1991)
5. Amari, S.: Information geometry of the EM and em algorithms for neural networks. Neural Networks **8**(9), 1379–1408 (1995)
6. Burns, A.R., Bowden, R.A., MacDonell, S.D., Walker, D.C., Odebunmi, T.O., Donnachie, E.M., Simon, S.I., Entman, M.L., Smith, C.W.: Analysis of tight junctions during neutrophil transendothelial migration. J. Cell Sci. **113**, 45–57 (2000)
7. Carmo, M.P.D.: Riemannian Geometry. Birkhauser, Boston (1992)
8. Choi, C.K., English, A.E., Jun, S.-I., Kihm, K.D., Rack, P.D.: An endothelial cell compatible biosensor fabricated using optically thin indium tin oxide silicon nitride electrodes. Biosensors and Bioelectronics **22**, 2585–2590 (2007)
9. Chentsov, N.N.: Statistical Decision Rules and Optimal Inference. AMS, Providence, RI (1982)
10. Csiszar, I., Cover, T.M., Choi, B.S.: Conditional limit theorems under Markov conditioning. IEEE Trans. Inform. Theory **IT-33**, 788–901 (1987)
11. Ellis, C.A., Tiruppathi, C., Sandoval, R., Niles, W.D., Malik, A.B.: Time course of recovery of endothelial cell surface thrombin receptor (Par-1) expression. Am. J. Physiol. (Cell Physiol.) **276**, C38–C45 (1999)
12. English, A.E., Squire, J.C., Bodmer, J.E., Moy, A.B.: Endothelial cell electrical impedance parameter artifacts produced by a gold electrode and phase sensitive detection. IEEE Trans. BioMed. Eng. **54**, 863–873 (2007)
13. Gainor, J.P., Morton, C.A., Roberts, J.T., Vincent, P.A., Minnear, F.L.: Platelet-conditioned medium increases endothelial electrical resistance independently of Camp/Pka and Cgmp/Pkg. Am. J. Physiol. Heart Circ. Physiol. **281**, H1992–H2001 (2001)
14. Giaever, K.: Micromotion of endothelial cells measured electrically. Cell Biol. - Proc. Natl. Acad. Sci. USA **88**, 7896–7900 (1991)
15. Giaever, I., Keese, C.R.: Correction: micromotion of mammalian cells measured electrically. Proc. Natl. Acad. Sci. USA **90**, 1634 (1993)
16. Johnson, R.A., Wichern, D.W.: Applied Multivariate Statistical Analysis. Prentice-Hall, New Jersey (1982)
17. Kataoka, N., Iwaki, K., Hashimoto, K., Mochizuki, S., Ogasawara, Y., Sato, M., Tsujioka, K., Kajiya, F.: Measurements of endothelial cell-to-cell and cell-to-substrate gaps and micromechanical properties of endothelial cells during monocyte adhesion. Proc. Natl. Acad. Sci. **99**, 15638–15643 (2002)
18. Lo, C.-M., Ferrier, J.: Impedance analysis of fibroblastic cell layers measured by electric cell–substrate impedance sensing. Phys. Rev. E **57**, 6982–6987 (1998)
19. Lo, C.-M., Keese, C.R., Giaever, I.: Impedance analysis of Mdck cells measured by electric cell–substrate impedance sensing. Biophys. J. **69**, 2800–2807 (1995)
20. Moy, A.B., VanEngelenhoven, J., Bodmer, J., Kamath, J., Keese, C., Giaver, I., Shasby, S., Shasby, D.M.: Histamine and thrombin modulate endothelial focal adhesion through centripetal and centrifugal forces. J. Clin. Invest. **97**, 1020–1027 (1996)
21. Moy, A.B., Winter, M., Kamath, A., Blackwell, K., Reyes, G., Giaever, I., Keese, C., Shasby, D.M.: Histamine alters endothelial barrier function at cell–cell and cell–matrix sites. Am. J. Physiol. Lung. Cell Mol. Physiol. **278**, L888–L898 (2000)
22. Nagaoka, H., Amari, S.: Differential geometry of smooth families of probability distributions. Univ. Tokyo, Tokyo, Japan, METR, 82-7 (1982)
23. Noiri, E., Lee, E., Testa, J., Quigley, J., Colflesh, D., Keese, C.R., Giaever, I., Goligorsky, M.S.: Podokinesis in endothelial cell migration: role of nitric oxide. Am. J. Physiol. **274**, C236–C244 (1998)
24. Phelps, J.E., DePaola, N.: Spatial variations in endothelial barrier function in disturbed flows in vitro. Am. J. Physiol. Heart Circ. Physiol. **278**, H469–H476 (2000)
25. Press, W.H., Bettering, W.T., Teukolsky, S.A., Flannery, B.P.: Numerical Recipes in C++ the Art of Scientific Computing. Cambridge University Press, Cambridge (2002)
26. Rao C., R.: Information and accuracy attainable in the estimation of statistical parameters. Bull. Calcutta. Math. Soc. **37**, 81–91 (1945)
27. Shasby, M.D., Shasby, S.S.: Effects of calcium on transendothelial albumin transfer and electrical resistance. J. Appl. Physiol. **60**, 71–79 (1986)

28. Shasby, M.D., Shasby, S.S., Sullivan, J.M., Peach, M.J.: Role of endothelial cell cytoskeleton in control of endothelial permeability. Circ. Res. **51**, 657–661 (1982)
29. Tanaka, T.: Information geometry of mean field approximation. Neural Comput. **12**, 1951–1968 (2000)
30. Tiruppathi, C., Malik, A.B., Vecchio, P.J.D., Keese, C.R., Giaever, I.: Electrical method for detection of endothelial cell shape change in real time: assessment of endothelial barrier function. Proc. Natl. Acad. Sci. USA **89**, 7919–7923 (1992)
31. Tschugguel, W., Zhegu, Z., Gajkzik, L., Maier, M., Binder, B.R., Graf, J.: High precision measurement of electrical resistance across endothelial cell monolayers. Pflugers Arch. - Eur. J. Physiol. **430**, 145–147 (1995)
32. Warner, F.W.: Foundations of Differential Manifolds and Lie Groups. Springer, New York (1983)
33. Wegener, J., Zink, S., Rosen, P., Galla, H.-J.: Use of electrochemical impedance measurements to monitor beta-adrenergic stimulation of bovine aortic endothelial cells. Pflugers. Arch. - Eur. J. Physiol. **437**, 925–934 (1999)